Control Engineering Practice 103 (2020) 104612

Contents lists available at ScienceDirect

Control Engineering Practice

journal homepage: www.elsevier.com/locate/conengprac

A gain scheduling approach to improve pressure control in water distribution networks

Giacomo Galuppini *, Enrico Creaco, Lalo Magni

Dipartimento di Ingegneria Civile e Architettura, University of Pavia, Pavia 27100, Italy

ARTICLE INFO

Keywords:
WDN
Pressure control
Gain scheduling
PI
Smith predictor

ABSTRACT

Real time pressure control is a common technique adopted to face the problem of leakage reduction in water distribution networks. Recently, in the context of *Water 4.0*, the spread of wired water distribution networks has opened new possibilities in terms of sensing and communication, resulting in the possibility of adopting higher sampling rates and consequently higher closed-loop bandwidths for the control system. While this could be exploited to improve the performance, it has also drawn the attention of the fundamental question of closed-loop stability, which was seldom considered in a systematic way, especially in the hydraulic community. This works aims to combine some recent results in term of design of frequency domain controllers with a gain scheduling approach, to account and compensate for the main nonlinearities affecting the system under control, and to preserve stability and robustness of the closed-loop in a wide operating region. The approach is validated by means of simulated experiments performed on a detailed dynamic model of the water distribution network. In addition, the gain scheduling approach can improve the overall performance of the control scheme and allows avoiding heavy retuning of the regulator when applied to the nonlinear system.

1. Introduction

Real Time Control (RTC) of service pressure plays a fundamental role in the context of Water Distribution Networks (WDNs) management, allowing for leakage reduction (Creaco & Walski, 2017; Farley & Trow, 2003), pipe burst abatement (Creaco & Walski, 2017; Lambert, Fantozzi, & Thornton, 2013; Thornton & Lambert, 2006) and overall infrastructure life extension. The WDN is first subdivided in homogeneous pressure zones (Walski et al., 0000). On this basis, hierarchical control schemes are developed, with high-level optimal controllers defining the pressure setpoints for the different pressure zones, according to an economic cost–benefit evaluation over the whole network, and RTC controllers working as low-level controllers to ensure regulation to the assigned setpoint (Cembrano, Wells, Quevedo, Pérez, & Argelaguet, 2000; Grosso, Maestre, Ocampo-Martinez & Puig, 2014; Grosso, Ocampo-Martínez, Puig & Joseph, 2014; Grosso, Velarde, Ocampo-Martinez, Maestre, & Puig, 2017; Ocampo-Martinez, Barcelli, Puig, & Bemporad, 2012; Ocampo-Martinez, Puig, Cembrano, & Quevedo, 2013; Toro, Ocampo-Martínez, Logist, Impe, & Puig, 2011). Recently, the spread of wired water distribution networks, promoted by the *Water 4.0* approach, is attracting new interest on the design of low level controllers. In fact, in wired WDNs, sensors and actuators are connected by wire to control units: this allows developing new control approaches working with high sampling rates. Some recent works (Fontana, Giugni, Glielmo, Marini, & Verrilli, 2017; Fontana, Giugni, Glielmo, Marini, & Zollo, 2017; Galuppini, Creaco, Toffanin, & Magni, 2019) try to investigate this approach and compare it to more traditional control strategies (Campisano, Creaco, & Modica, 2009; Campisano, Modica, Reitano, Ugarelli, & Bagherian, 2016; Campisano, Modica, & Vetrano, 2011; Creaco, Campisano, & Modica, 2018; Creaco & Franchini, 2013), to understand how to exploit the new communication possibilities at best. The design of such control algorithms results particularly challenging, due to the complexity of the nonlinear system under control, and the topic of guaranteed closed-loop stability, which was previously disregarded by the hydraulic community, is getting more and more attention (Galuppini, Magni, & Creaco, 2020; Janus & Ulanicki, 2017, 2018). In particular, Fontana, Giugni, Glielmo, Marini, and Verrilli (2017) and Galuppini et al. (2019) propose a model-based frequency domain approach, with regulators based on a linear, local model of the system dynamics around the working point. The issue of stability is faced by providing robustness margins against gain and phase variations. Galuppini et al. (2020) further investigates the problem of stability, and demonstrates that a poor description of the high frequency behaviour of the system, together with the strong gain nonlinearity affecting the Pressure Control Valves (PCVs) exploited as actuators, may result in highly overestimated robustness margins and, eventually, in closed-loop instability as the process moves from its nominal working point. The aim of this paper is to improve the design methodology originally developed in Galuppini et al. (2019),

* Corresponding author.
E-mail address: giacomo.galuppini01@ateneopv.it (G. Galuppini).

https://doi.org/10.1016/j.conengprac.2020.104612
Received 30 January 2020; Received in revised form 14 August 2020; Accepted 15 August 2020
Available online 26 August 2020
0967-0661/

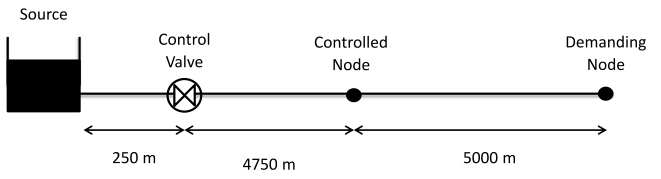

Fig. 1. Case Study A: topology of the water distribution system (Galuppini et al., 2019).

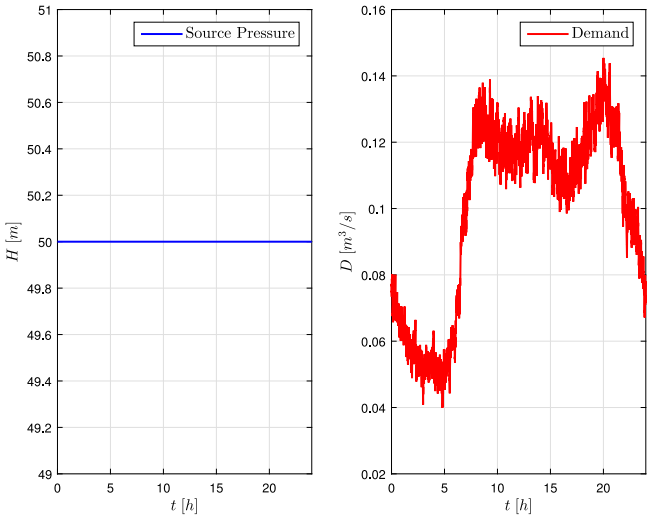

Fig. 2. Case Study A: source pressure and demand profile.

to explicitly account and compensate for the main static nonlinearities characterising the process under control. This is achieved by means of a proper choice of the control variable (inspired by Creaco, 2017), a nonlinearity inversion block, and a gain scheduling approach. The gain scheduling policy is further extended to better manage the *regulation error vs cost of control* trade-off at different operating points of the system. The correctness of the approach is verified by means of closed-loop simulations, performed on a detailed model of two different WDN topologies and different user demand scenarios. This paper is organised as follows: Section 2 describes the different case studies adopted for simulations while Section 3 reports the details of their numerical modelling; Section 4 discusses the control methodology and Section 5 its application to the case studies. Finally, a detailed discussion of the results, including a comparison with similar algorithms, is given in Section 6, while the conclusions are reported in Section 7.

2. Case studies

The control algorithms developed in this work are tested over two different WDN topologies, characterised by very different dynamic behaviours. For sake of comparison, reference is made to the same case studies adopted in Galuppini et al. (2019, 2020), which can be consulted for further details. For both case studies, the control goal is the regulation to the setpoint of the measured pressure at the critical node, in presence of process disturbances generated by the time varying users' demand and, for Case Study B only, time-varying source pressure head. Moreover, the performance of the control algorithms are evaluated by means of the same performance metrics adopted in Galuppini et al. (2019, 2020) and summarised in the following of this paper.

Case Study A, depicted in Fig. 1, consists of a simple water distribution system, with a single source node, connected to a single demanding node by means of a pipe. No leakage is considered in this system.

The time behaviours of source pressure head and demand are depicted in Fig. 2. In addition, to stress the robustness of regulation,

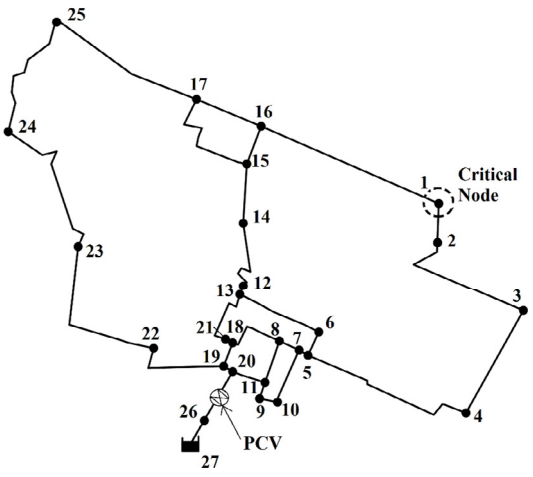

Fig. 3. Case Study B: topology of the WDN (Creaco, 2017).

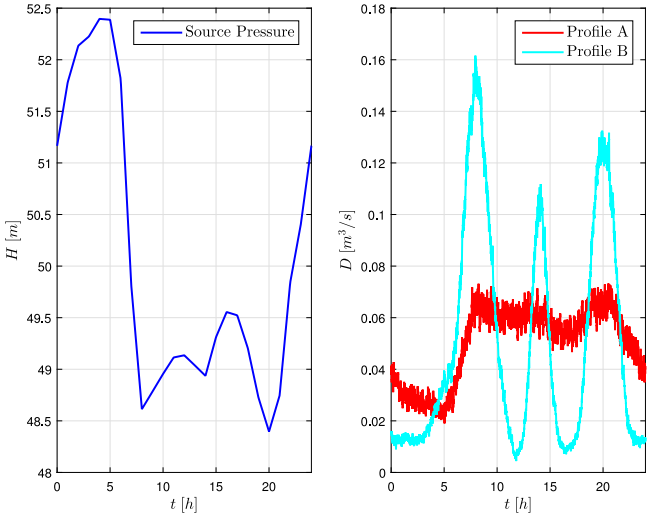

Fig. 4. Case Study B: source pressure and demand profiles.

simulations are repeated introducing different offsets in the demand profile. The offsets range in the interval $[-0.03; 0.05]$ [m^3/s], to account for possible seasonal variation of the demand.

Case Study B, depicted in Fig. 3, is represented by the skeletonised WDN of the Italian town of Castelfranco Emilia (about 30,000 inhabitants). A leakage percentage of 20% is considered in this system. Two different demand patterns are considered for this case study, leading to two different trends of the total WDN demand (see Fig. 4): a flatter trend (profile A) and a more peaked trend (profile B), with the aim of stressing more the robustness of regulation. Note that demand profiles A and B share the same average values for each single demand profile. The source pressure head profile is reported in Fig. 4 as well.

In both cases, nodal demands are generated at the temporal scale of 1 s, making use of statistic models for demand pulse generation (Creaco, Campisano, Franchini, & Modica, 2017). Additionally, the speed of both PCVs is limited, for safety reasons, to 0.01 s^{-1} for Case Study A and to 0.0033 s^{-1} for Case Study B.

3. Numerical model

Unsteady flow modelling (Creaco et al., 2017; Streeter, Wylie, & Bedford, 1998) allows a proper analysis of the hydraulic transients due to rapid nodal demand and/or valve setting variations, and is therefore

adopted in this work to develop a simulated environment for the WDNs considered as case studies.

For a generic pipe of a WDN, the one-dimensional unsteady flow equations take the form:

$$\begin{aligned} &\frac{\partial h_p}{\partial x} + \frac{1}{gA}\frac{\partial Q_p}{\partial t} + J_p = 0 \\ &\frac{\partial h_p}{\partial t} + \frac{c^2}{gA}\frac{\partial Q_p}{\partial x} + \frac{c^2 q}{gA} = 0 \end{aligned} \tag{1}$$

where h_p [m] and Q_p [m^3/s] are the pressure head and the flow discharge along the pipe, x [m] is the position along the pipe, t [s] is time, A [m^2] is the pipe cross-section area, g [m/s^2] is the gravity acceleration constant, c [m/s] is the wave celerity, q [m^2/s] is the leakage outflow per unit of length, J_p is the friction slope.

The wave celerity c can be related to physical quantities of water and of the pipe as follows:

$$c = \left(\frac{\frac{\epsilon}{\zeta}}{1 + \frac{\epsilon d}{Es}} \right)^{\frac{1}{2}} \tag{2}$$

where ϵ [Pa] and ζ [kg/m^3] are water bulk modulus and density; E [Pa], d [m] and s [m] are pipe modulus of elasticity, diameter and thickness.

Pipe friction slope can be computed as:

$$J_p = 10.29 \frac{n^2 |Q_p| Q_p}{d^{5.33}} \tag{3}$$

where n [$s/m^{\frac{1}{3}}$] is the Gauckler–Manning coefficient.

To improve the accuracy of the model, a *pressure-driven* approach is adopted, as described in Ciaponi, Franchioli, Murari, and Papiri (2015), and pipe friction slopes increased using the correction proposed by Pezzinga in Pezzinga (2000), to account for the unsteady flow effects on pipe friction slopes.

Finally, the presence of leakage from WDN pipes is considered by means of the following outflow q:

$$q = \alpha_{leak} h_p^{\gamma} \tag{4}$$

where α_{leak} [m/s] and γ [−] are the leakage coefficient and exponent, respectively. As for leakage evaluation, exponent γ is set to 1, typical value for plastic pipes (Van Zyl & Cassa, 2013). Coefficient α_{leak} [−] is set to 0 and 9.4 10^{-9} m/s to obtain a leakage percentage rate of 0% and 20%, in the two case studies, respectively.

The effect of the control valve is modelled by considering no link at the valve site and setting nodal inflow at the upstream end at:

$$Q_{up} = \sqrt{\frac{2g}{\xi(\alpha)}} A \sqrt{\Delta H_{valve}} \tag{5}$$

and the inflow at the downstream end is set, instead, to:

$$Q_{down} = Q_{up} \tag{6}$$

where A [m^2] is the valve cross-section area, g [m/s^2] is the gravity acceleration constant, ξ is the valve head loss coefficient, ΔH_{valve} is the head drop in the valve and α is the valve closure setting, ranging from 0 (fully open) to 1 (fully closed). The valve head loss coefficient is a growing function of α. This function is typically made available by the valve manufacturer.

Realistic measurement noises $n_h(t)$ and $n_q(t)$ are present, acting respectively on the pressure $h(t)$, and on the flow at the valve site $Q(t)$.

3.1. Model implementation

In the model implementation, unsteady flow equations are solved by relying on the method of the characteristics (Streeter et al., 1998). Network pipes are discretised with spatial steps Δx, and the hydraulic variables of interest computed at each time integration step Δt. Note that Δx and Δt must fulfil the Courant condition (Streeter et al., 1998):

$$c \frac{\Delta t}{\Delta x} \leq 1 \tag{7}$$

The discretised unsteady flow equations are coupled with the continuity equation, applied to each node of the WDN. At each integration time step, suitable boundary conditions are assigned in correspondence to source and demanding nodes, where fixed total pressure head and demands are prescribed, respectively. In case of the pressure control valve, given the valve closure α, boundary conditions for the upstream and downstream pipes, Q_{up} and Q_{down} respectively, are computed by solving a system of equations composed of the valve equation (5), the valve continuity equation (6), the positive characteristic line related to the last section of the upstream pipe, and the negative characteristic line related the first section of the downstream pipe. This approach demonstrated to be robust and provide very similar results when compared to modelling methodologies based on localised head loss and equivalent roughness coefficients.

4. Control algorithm design methodology

This section is devoted to the description of the control algorithm design methodology. In particular, the design consists of three main phases:

- Nominal design of the regulator.
- Definition of a gain scheduling policy to compensate for process gain nonlinearities.
- Definition of an additional gain scheduling policy to balance between cost of control and regulation error at different working points.

Each step of the procedure is described in detail in the following subsections.

4.1. Nominal design

The first phase of the procedure is the design of a regulator around the nominal working point (WP) of the system. The nominal design takes advantage of the considerations reported in Galuppini et al. (2019, 2020), and is based on the following steps:

- Definition of the nominal WP of the system.
- Identification of a linear, local model of high order to accurately describe the dynamics of the system (Galuppini et al., 2020).
- Design of a Filtered Proportional–Integral (FPI) regulator with Smith predictor (SP) for process delay compensation (Galuppini et al., 2019).

4.1.1. Working point

The nominal WP of the system can be found experimentally by means of simulations. For both case studies, the curve $\xi(\alpha(t))$ introduced in Section 3 is known and invertible. It is then possible to consider the Multi-Input Multi-Output (MIMO) system with the following input signals:

- $\xi(\alpha(t))$, the local loss coefficient, function of the valve closure ([−]).
- $H(t)$, the source pressure head ([m]).
- $D_i(t)$, the water demand ([m^3/s]) at node i.

The outputs are

- $h(t)$, the pressure measured at the desired node of the WDN ([m]).
- $Q(t)$ the flow measured at the valve site ([m^3/s]).

Let $\xi(\alpha(t))$ be control variable, $H(t)$ and $D_i(t)$ be stochastic disturbances acting on the process. Fig. 2 shows the profile of $D(t)$ adopted for simulations with Case Study A. Fig. 4 shows instead the profiles for Case Study B, with $D(t)$ representing the overall demand of the WDN, i.e.:

$$D(t) = \sum_{i=1}^{N_{nodes}} D_i(t) \tag{8}$$

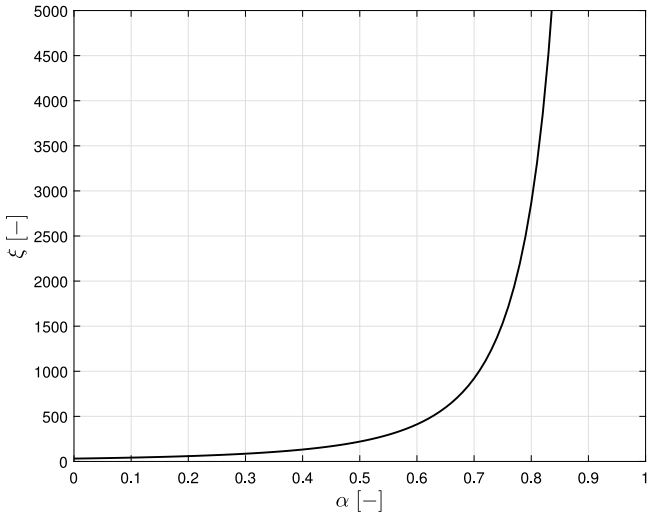

Fig. 5. The local loss coefficient ξ as function of the valve closure α.

where N_{nodes} is the number of demanding nodes in the WDN. The average values of typical $H(t)$ and $D_i(t)$ profiles are considered as input to the system for the definition of the WP. Note that this information is usually available to the WDN manager. Under these assumptions, simulations allow definition of the value of ξ resulting in the desired pressure h_{sp}. Let the tuple $WP_A = (\overline{\xi}, \overline{H}, \overline{D}, \overline{h}, \overline{Q})$ represent the working point for Case Study A, and the tuple $WP_B = (\overline{\xi}, \overline{H}, \overline{D}_1, \ldots, \overline{D}_{N_{nodes}}, \overline{h}, \overline{Q})$ represent the working point for Case Study B.

Remark. the choice of $\xi(\alpha(t))$ as control variable, opposed to $\alpha(t)$, is motivated by the strong nonlinearity of the $\xi(\alpha(t))$ curve. An example, related to case Study A, is reported in Fig. 5. As underlined in Galuppini et al. (2020), when the system moves far away from its nominal WP, with $\alpha \approx 1$ in particular, the increase in the process gain can exceed the robustness margin associated with the control design, therefore resulting in instability of the closed-loop system. To overcome this problem, since the $\xi(\alpha(t))$ curve is typically available and invertible, it is possible to exploit $\xi(\alpha(t))$ as control variable and introduce a nonlinearity inversion block in the loop to compute, instant by instant, the value of $\alpha(t)$ resulting in the desired $\xi(\alpha(t))$. Such value of $\alpha(t)$ can be used to control the PCV.

4.1.2. Dynamic models

The synthesis of regulators is based on a linear dynamic model relating $\xi(\alpha(t))$ to the pressure $h(t)$. Such model which can be obtained by applying black-box identification to simulated step response data collected from the simulator. In particular, a preliminary study (Galuppini et al., 2020) suggests that standard low order models do not allow a proper description of the high frequency behaviour of the system, which is characterised by multiple resonance peaks associated with low value of damping. In view of this consideration, a 9th order transfer function with delay is used to describe the dynamics of the system around the equilibrium. Let this model be denoted in general as $G(s)$, with s the *Laplace* variable. Let also $G_a(s)$ and $G_b(s)$ be the models for Case Study A and B, respectively. The identification phase is set-up as follows: first, the system is brought to its nominal WP, then a step variation of ξ is applied to the system and the variation signals $\delta\xi(t) = \xi(t) - \overline{\xi}$ and $\delta h(t) = h(t) - \overline{h}$ constructed as input–output data. Matlab Identification Toolbox (Ljung, 1991) can be used to estimate the parameters of $G(s)$, to provide the best fit between model prediction and identification data. Finally, the model prediction is compared against new simulations of step responses of the WDN. Examples of $G(s)$ (from Case Study A) are reported in Fig. 6.

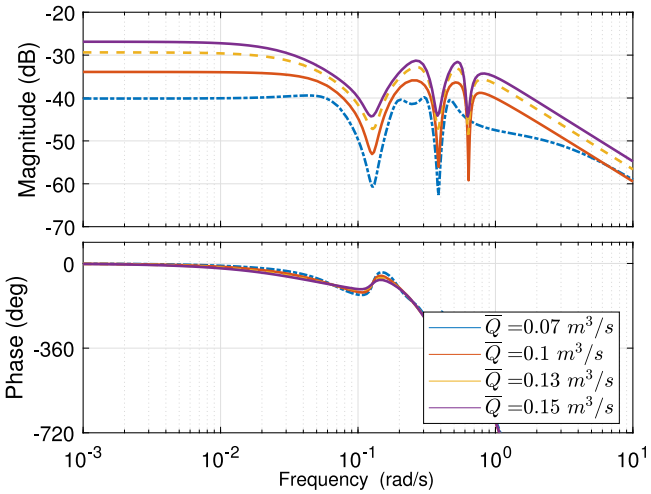

Fig. 6. Case Study A. Bode diagrams of $G_a(s)$ obtained around various WPs characterised by demand $\overline{Q} = 0.07\,\mathrm{m}^3/\mathrm{s}$ (blue dotted line), $\overline{Q} = 0.1\,\mathrm{m}^3/\mathrm{s}$ (orange solid line), $\overline{Q} = 0.13\,\mathrm{m}^3/\mathrm{s}$ (yellow dashed line), $\overline{Q} = 0.15\,\mathrm{m}^3/\mathrm{s}$ (violet solid line), with source pressure $\overline{H} = 50$ m. (For interpretation of the references to colour in this figure legend, the reader is referred to the web version of this article.)

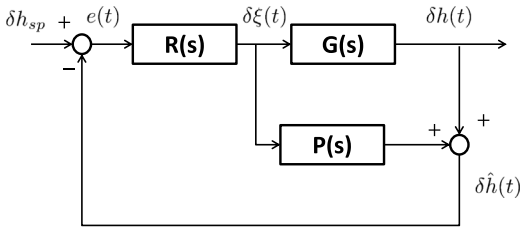

Fig. 7. Control scheme with Smith predictor for the linearised design framework.

The transfer function $G(s)$ allows both tuning the regulator transfer function and developing a Smith predictor for delay compensation, as described in the following subsection.

4.1.3. Control design

The main goal is regulation to the setpoint h_{sp} of the pressure $h(t)$, in presence of process disturbances generated by the effect of exogenous inputs $H(t)$ and $D_i(t)$. In this situation, reference can be made to a Single-Input Single-Output (SISO) system, whose behaviour around the working point is described by $G(s)$.

A Smith Predictor is first introduced to compensate for the effect of the pure delay present in $G(s)$. In particular, let

$$G(s) = G'(s)e^{-s\tau} \tag{9}$$

where $G'(s)$ is the rational part of the transfer function. Then, with reference to the control scheme in Fig. 7, it is possible to neglect the presence of the pure delay $e^{-s\tau}$ in the design of the regulator transfer function $R(s)$ when

$$P(s) = (1 - e^{-s\tau})G'(s) \tag{10}$$

The effect of the scheme is to obtain a feedback with a *prediction* $\delta\hat{h}(t) = \delta h(t + \tau)$ of the controlled variable $\delta h(t)$.

Regulators are then synthesised requiring the closed-loop bandwidth to be the largest possible, while providing at the same time attenuation of high frequency resonance peaks of $G(s)$ and robustness to gain and phase variations. A static precision requirement is also present. To this end, A PI regulator with an additional low-pass filter proved to be an effective design tool (Galuppini et al., 2019). Let $R_{pi}(s)$

be the PI transfer function, as reported in (11).

$$R_{pi}(s) = \mu_r \frac{1 + sT_i}{s} = K_i \frac{1 + s\frac{K_p}{K_i}}{s} \tag{11}$$

with K_p the proportional gain, K_i the integral gain and $T_i = K_p/K_i$ the integral time constant. The static gain of the transfer function μ_r coincides with K_i.

Let then $R_f(s)$ be the filter transfer function, as reported in (12).

$$R_f(s) = \frac{(1 + sT_d)}{(1 + sT_f)} \tag{12}$$

Finally, the overall regulator transfer function $R(s)$ is given in (13).

$$R(s) = R_f(s)R_{pi}(s) \tag{13}$$

Note that $R_f(s)$ has unitary static gain, so that μ_r coincides with the gain of the overall regulator.

The presence of the filter is motivated by the need to attenuate the high frequency resonance peaks of $G(s)$. Let ω_{rp} be the angular frequency associated to the resonance peak of $G(s)$ located at the lowest frequency. Then, a possibility is to set:

$$T_d = \frac{1}{5}\frac{1}{\omega_{rp}} \quad T_f = 20T_d \tag{14}$$

As far as R_{pi} is concerned, let T_p be the time constant associated to the lowest frequency pole of $G(s)$ with null imaginary part. One can then set:

$$T_i = T_p \quad \mu_r = \frac{\omega_c}{\mu_g} \tag{15}$$

where ω_c is the desired closed-loop bandwidth expressed in rad/s.

At this point, ω_c is the only free design parameter, and must be chosen so that $\omega_c < \omega_{rp}$ and to provide robustness margins against gain and phase uncertainties. Note that, in case $\frac{1}{T_f} < \omega_c$, the effective closed-loop bandwidth is going to be smaller than required due to the effect of the pole associated with time constant T_f. Finally, nominal stability of the closed-loop must be proved, e.g. by means of *Bode criterion* (Seborg, Mellichamp, Edgar, & Doyle, 2010).

The rationale behind this tuning procedure is to obtain a loop function $L(s) = G(s)R(s)$ characterised by the largest closed-loop bandwidth possible and de-amplified high frequency resonance peaks from $G(s)$. As discussed in Galuppini et al. (2020), this shaping of the loop function allows both improving the robustness of the design and reduction of the control sensitivity outside of the closed-loop bandwidth, thus resulting in a reduced cost of control associated with pressure regulation.

Note that the control action is characterised by a saturation, since the valve closure α ranges in the interval $[0; 1]$, or, more in general in the interval $[\alpha_{min}; \alpha_{max}]$, with $0 \leq \alpha_{min} < \alpha_{max} < 1]$. To cope with this saturation, it is necessary to introduce an antiwindup implementation of $R_{pi}(s)$, which features an integral action, as described more in detail in Section 4.3.2.

The regulator is finally implemented in a discrete-time way, by exploiting the full capability of the measurement system in terms of sampling time, which results in $T_s = 1$ s. Discretisation is performed with *Tustin* method to guarantee that the stability is preserved (all asymptotically stable/stable continuous time poles are respectively mapped into asymptotically stable/stable discrete time poles).

4.2. Gain scheduling policy

This Section discusses two different gain scheduling policies which can be introduced in the control design to improve its robustness against process nonlinearity and improve its overall performance.

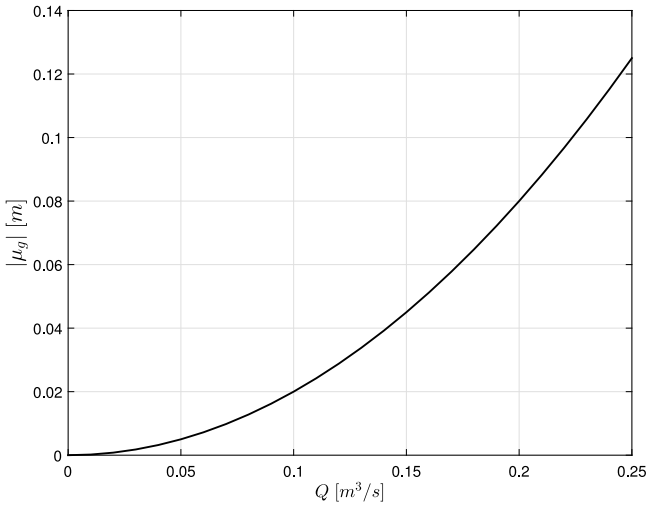

Fig. 8. Absolute value of the gain of the linearised system μ_g as function of the flow Q.

4.2.1. Gain scheduling for nonlinearity compensation

Once a nominal design of the regulator is available, a gain scheduling policy can be introduced to account for a further gain nonlinearity affecting the process. In particular, Eq. (5) shows a dependence of the pressure loss induced by the valve on the flow through the valve itself Q. It is fact possible to write:

$$\Delta H_{valve} = \frac{Q^2}{\sqrt{2gA}}\xi(\alpha) \tag{16}$$

Moreover, Eq. (16) shows a dependence on Q^2. The presence of this nonlinearity can also be demonstrated by repeating the model identification procedure around different WPs, characterised by different valve flow values. Fig. 8 depicts the absolute value of the process gain as function of the flow and highlights the quadratic dependence. The same procedure was applied to obtain the Bode diagrams depicted in Fig. 6. To compensate for this effect, the regulator gain can be adjusted to maintain the desired closed-loop bandwidth when the process moves far away from the nominal flow associated to the nominal flow $\overline{Q}$. This can be obtain by computing, at each time instant, $\mu_r^{gsq}(t)$, the adapted regulator gain, as follows:

$$\mu_r^{gsq}(t) = \mu_r \left(\frac{\overline{Q}}{Q(t)}\right)^2 \tag{17}$$

Similarly, the Smith Predictor can be adjusted by setting, at each time instant, the gain of $G'(s)$ as follows:

$$\mu_g^{gsq}(t) = \mu_g \left(\frac{Q(t)}{\overline{Q}}\right)^2 \tag{18}$$

Note that, as discussed more in detail in the following of this work, the value of the pure delay affecting the process is related to the topology of the WDN and to the celerity of pressure waves, which do not depend on the WP. No adaptation strategy for the time delay is therefore introduced in the Smith predictor.

In the following of this work, let refer to this gain scheduling policy as $GS - Q$.

Fig. 9 shows the Bode diagrams of the transfer functions reported to the nominal gain by the application of $GS - Q$. Note that the variations in static gain due to the different flow values is correctly compensated. Also note that the damping of the resonance peaks is higher at higher values of the flow. This is consistent with the fact that energy loss per unit of length also increases as the flow increases (Pezzinga, 2000; Streeter et al., 1998).

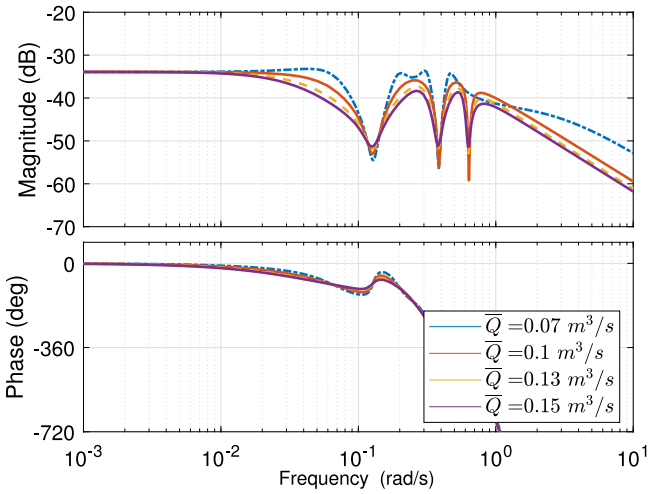

Fig. 9. Case Study A. Bode diagrams of $G_a(s)$ obtained around various WPs, adjusted with the $GS-Q$ gain scheduling policy. WPs are characterised by demand $\overline{Q} = 0.07\,\mathrm{m}^3/\mathrm{s}$ (blue dotted line), $\overline{Q} = 0.1\,\mathrm{m}^3/\mathrm{s}$ (orange solid line), $\overline{Q} = 0.13\,\mathrm{m}^3/\mathrm{s}$ (yellow dashed line), $\overline{Q} = 0.15\,\mathrm{m}^3/\mathrm{s}$ (violet solid line), with source pressure $\overline{H} = 50$ m. (For interpretation of the references to colour in this figure legend, the reader is referred to the web version of this article.)

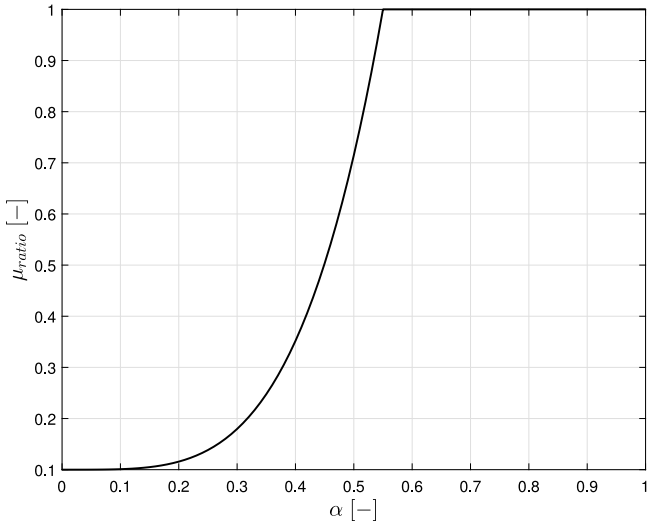

Fig. 10. Example of gain scheduling policy $GS-\alpha$ with $\alpha^* = 0.55$, $\mu^*_{ratio} = 0.1$ and $p = 4$.

Remark. the control approach based on ξ as control variable, associated with the $GS-Q$ policy, aims to maintain the robustness margins unchanged during the operations. However, the $\xi(\alpha)$ curve is typically derived experimentally by manufacturers, and can be affected by uncertainty. In addition, some hysteresis may be present in the operation of PRC valves. It is therefore important to provide reasonable nominal stability margins which could cope with such uncertainties.

4.2.2. Gain scheduling for regulation error versus cost of control trade-off

The gain scheduling policy introduced in the previous section allows compensation of the gain nonlinearity of the process related to the flow through the valve Q. At this point, the main static nonlinearities affecting the system are explicitly considered in the design of the control scheme, with the aim of maintaining the loop function design as constant as possible throughout the different working points of the WDN. Still, it is important to underline that, when the operating point of the WDN moves at high flow values, α assumes values close to zero. In this region, the curve $\xi(\alpha)$ becomes almost flat, meaning that even a small variation of the control signal ξ requires a wide variation of α to be realised, thus resulting in a very high cost of control associated with high flow conditions. To keep into account this behaviour, it is possible to introduce a further gain scheduling policy to reduce the closed-loop bandwidth in case of high flow, to obtain a better balance in the regulation error versus cost of control trade-off. In particular, it is possible to modify Eq. (17) to introduce a multiplicative factor $\mu_{ratio}(\alpha(t))$ depending on α, and compute the adapted regulator gain $\mu_r^{gs\alpha}(t)$, at each time instant, as follows:

$$\mu_r^{gs\alpha}(t) = \mu_{ratio}(\alpha(t))(\mu_r^{gsq}(t)) \tag{19}$$

The function $\mu_{ratio}(\alpha(t))$ defines the additional gain scheduling policy. In particular, assuming the nominal design of $R(s)$ to result in the maximum desired closed-loop bandwidth, it must hold $\mu_{ratio}(\alpha(t)) \in (0, 1]$.

In particular, in the context of this work, the function $\mu_{ratio}(\alpha(t))$ is defined as:

$$\mu_{ratio}(\alpha(t)) = \begin{cases} 1 & \forall \alpha(t) > \alpha^* \\ k * \alpha^{*p} + \mu^*_{ratio} & \forall \alpha(t) \le \alpha^* \end{cases} \tag{20}$$

$$k = \frac{1 - \mu^*_{ratio}}{\alpha^{*p}}; \tag{21}$$

with $\alpha^* \in [0; 1]$, $\mu^*_{ratio} \in (0; 1]$ and $p > 0$ are design parameters. In particular, μ^*_{ratio} represents the value of $\mu_{ratio}(\alpha)$ when $\alpha = 0$, p the power of increase of $\mu_{ratio}(\alpha)$ as $\alpha \to alpha^*$, α^* the upper limit of the gain scheduling policy, which affects the design only for $\alpha \in [0; \alpha^*]$. An example is reported in Fig. 10. In the following of this work, let refer to this gain scheduling policy as $GS-\alpha$.

Remark. note that, at this point, the overall control design includes, as free design parameters, ω_c, which defines the nominal closed-loop bandwidth, and the three parameters α^*, μ_{ratio} and p from $GS-\alpha$. On the other hand, $GS-Q$ is based on physical laws and does not require any additional tuning parameter.

In the following of this work, this algorithms will be referred to as $FPI-SP-gs$.

4.3. Control algorithm implementation

This section introduces some further remarks about the implementation of the control algorithm described in the previous Sections. A complete block scheme is depicted in Fig. 11.

4.3.1. Q and α filters

Note that both $GS-Q$ and $GS-\alpha$ are based on steady-state considerations about the process under control. However, in real life situations, the behaviour of the WDN is mainly driven by the demand at the different nodes, which show daily patterns as those depicted in Figs. 2 or 4. For this reason, to properly implement $GS-Q$, it is necessary to introduce a lowpass filter to remove the oscillations in $Q(t)$ arising from both high frequency demand oscillations and from the water hammer effect in the WDN pipes. In addition, part of such oscillations (depending on the control sensitivity function $Q(s) = R(s)L(s)/(1+L(s))$) are transferred to $\alpha(t)$. Therefore the same considerations hold for $GS-\alpha$. Let then $LP(s)$ be the transfer function of the lowpass filters used to remove oscillations in $Q(t)$ and $\alpha(t)$:

$$LP(s) = \frac{1}{1 + sT_{lp}} \tag{22}$$

with $T_{lp} = 180$ s the filter time constant used in this work. The filters are implemented in discrete time, with sampling times of 1 s for Case Study A, and 60 s for Case Study B, respectively. The gain scheduling policies $GS-Q$ and $GS-\alpha$ are then implemented by relying on $Q_{lp}(t)$ and $\alpha_{lp}(t)$, the lowpass filtered versions of, respectively, $Q(t)$ and $\alpha(t)$.

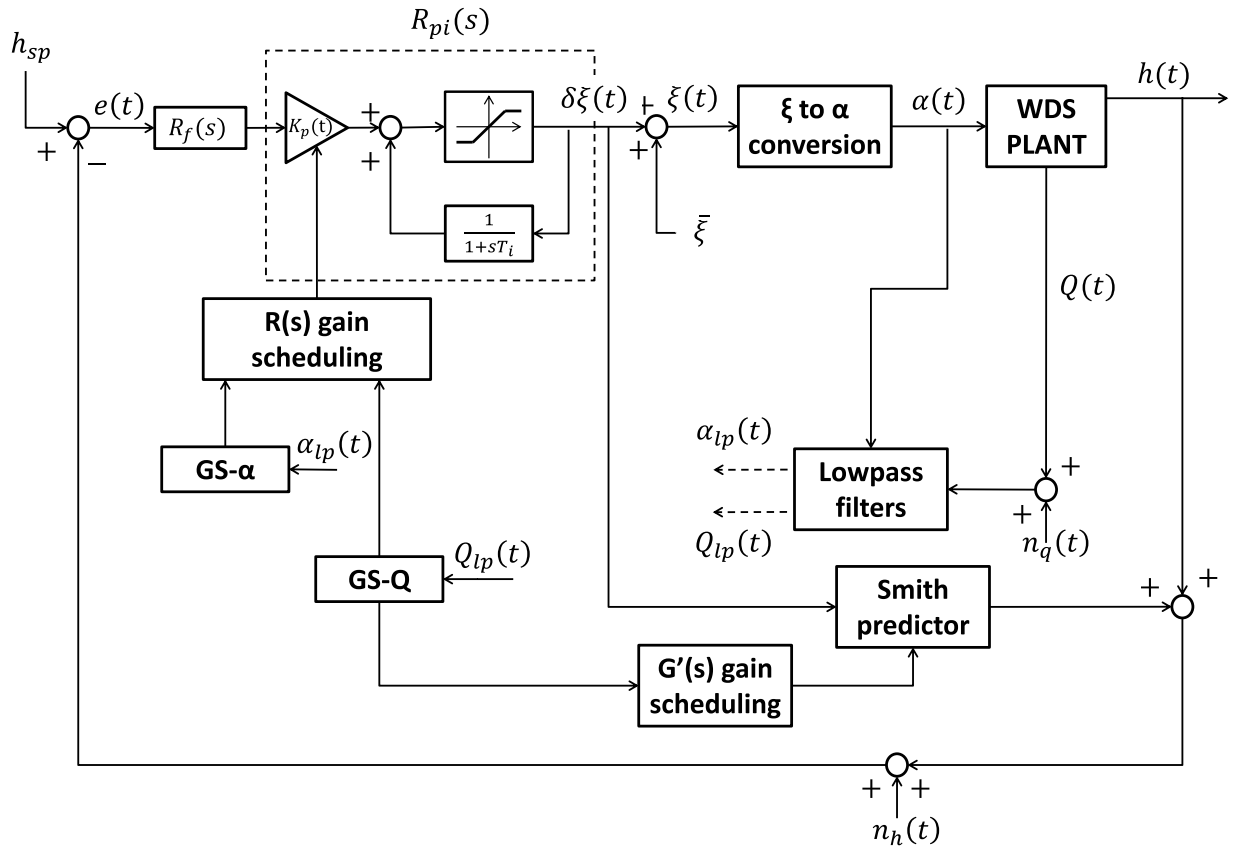

Fig. 11. Complete block scheme for the $FPI - SP - gs$ control algorithm including regulator with antiwindup implementation, Smith predictor, gain scheduling policies and lowpass filters.

4.3.2. Antiwindup implementation

As already introduced in Section 4.1.3, the presence of a saturation of the control action, combined with the integral action of the regulator, calls for an antiwindup implementation to avoid overshoots and undershoots that may eventually result in high pressure conditions of the WDN or emptying of the WDN. The antiwindup scheme adopted for this work is reported in Fig. 11, where a model of the saturation is introduced in the scheme to avoid spurious integration of control action which cannot reach the process.

The valve closure $\alpha(t)$ ranges in the interval $[0;1]$ due to physical limits. However, full closure is not typically admitted. Let therefore assume $\alpha(t) \in [\alpha_{min};\alpha_{max}]$, with $0 \leq \alpha_{min} < \alpha_{max} < 1]$. Consequently, a saturation is present on $\xi(\alpha(t))$. In particular, $\xi(\alpha(t)) \in [\xi_{min};\xi_{max}]$, with $\xi_{min} = \xi(\alpha_{min})$, and $\xi_{max} = \xi(\alpha_{max})$. Finally, since the regulator generates as control action the variation signal $\delta\xi(t) = \xi(t) - \overline{xi}$, this should be restricted to the interval $[\xi_{min} - \bar{\xi}; \xi_{max} - \bar{\xi}]$.

Note that, with this implementation of $R_{pi}(s)$, the only time varying parameter resulting from the application of a gain scheduling policy is $K_p(t)$, which can therefore be computed as follows:

$$K_p(t) = T_i \cdot \mu_r^{gs\alpha}(t) \tag{23}$$

5. Application

This Section is devoted to the application of the methodology to the two case studies introduced in Section 2. To quantify and compare the performances of the different control schemes, two metrics are introduced. All signals are sampled with a 1 s sampling time. Let k be the current discrete-time instant. Let $h(k)$ be the measured pressure, h_{sp} be the pressure setpoint, $\alpha(k)$ be the valve closure and $\Delta\alpha(k) = \alpha(k) - \alpha(k-1)$ be the variation of the valve closure over a single sampling time. Let $e(k) = h(k) - h_{sp}$ be the error of the controlled pressure head at time instant k. Then the metrics are defined as follows:

- $Mean|e(k)|$ [m]. The *regulation error*, which evaluates the proximity of the pressure to the desired setpoint.
- $\sum |\Delta\alpha(k)|$ [−]. The *cost of control*, which impacts on the energy required to perform regulation and on wear of actuators.

5.1. Case study A

The application of the proposed methodology to Case Study A is discussed in detail in this Section (see Eq. (24) in Box I).

5.1.1. Nominal design and gain scheduling policies

The control goal in Case Study A is to perform a pressure regulation at $h_{sp} = 29$ m at the controlled node, which is placed in the middle of the pipe. The first step of the methodology requires identification of the value of ξ resulting in the desired pressure, when the exogenous inputs acting on the system are the average value of the source pressure head $H(t)$ and the average value of the demand $D(t)$. This allows definition of the working point as follows:

$$WP_A = \begin{cases} \bar{\xi} = 871 \ (i.e.\ \bar{\alpha} = 0.694) \\ \overline{H} = 50 \text{ m} \\ \overline{D} = 0.1 \text{ m}^3/\text{s} \\ \bar{h} = 29 \text{ m} \\ \overline{Q} = 0.1 \text{ m}^3/\text{s} \end{cases} \tag{25}$$

Then a step response simulation around WP_A allows obtaining the input–output data for the identification of $G_a(s)$, as discussed in Section 4.1.2. The identification data and the corresponding model prediction are depicted in Fig. 12. Note that, for Case Study A, the pure delay is given by the time required by the pressure wave generated from the valve to reach the pressure sensor. The delay τ_a can be computed as:

$$\tau_a = \frac{L_{v-s}}{c} \tag{26}$$

$$G_a(s) = \frac{-0.007746s^8 - 0.001827s^7 - 0.004566s^6 - 0.0009353s^5 - 0.0006218s^4 - 9.963e-05s^3 - 1.721\times10-05s^2 - 1.362\times10-06s - 1.119\times10-07}{s^9 + 0.8226s^8 + 0.9946s^7 + 0.4754s^6 + 0.2612s^5 + 0.06681s^4 + 0.01795s^3 + 0.002027s^2 + 0.0002091s + 5.774\times10-06} e^{-11s} \quad (24)$$

Box I.

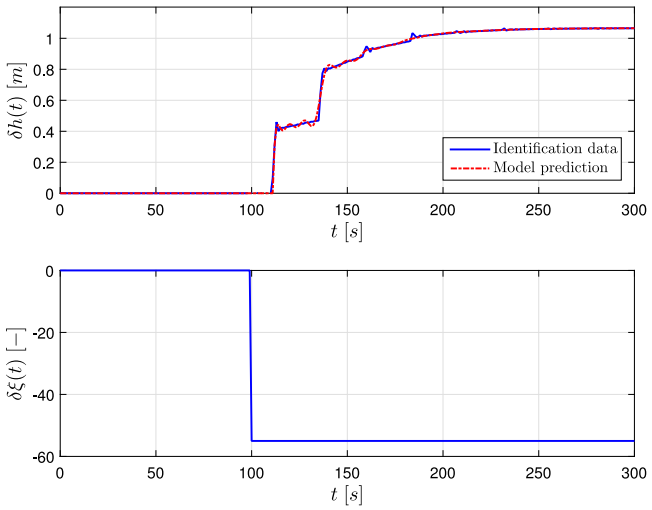

Fig. 12. Case Study A: model identification. Top: pressure variation $\delta h(t)$ (blue, solid line: identification data; red, dashed line: model prediction). Bottom: valve head loss coefficient variation $\delta\xi(t)$.

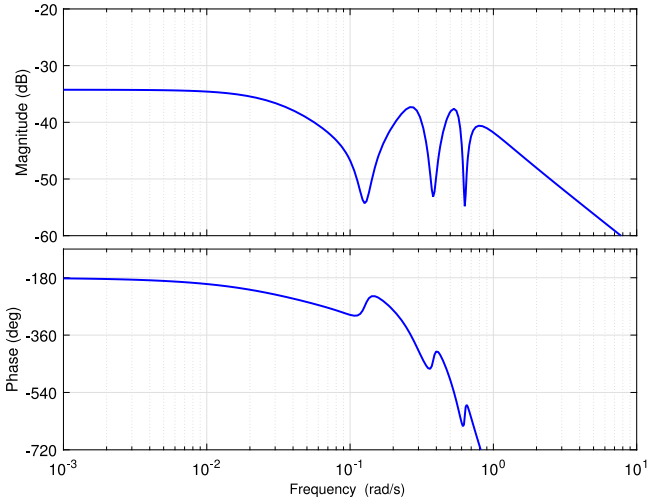

Fig. 13. Case Study A. Bode diagram of $G_a(s)$.

where L_{v-s} is the distance between the valve and the sensor and c is the celerity of the wave. In particular, it results:

$$\tau_a = 11 \text{ s} \quad (27)$$

The Bode diagram of $G_a(s)$ is depicted in Fig. 13, while its complete definition is reported in Eq. (24). First, a Smith predictor is designed on the basis of $G_a(s)$, then the nominal loop function $L_a(s)$, whose Bode diagram is depicted in Fig. 14, is designed according to methodology introduced in Section 4.1.3.

To this end, $R_f(s)$ can be obtained by deriving ω_{rp} from $G_a(s)$:

$$\omega_{rp} = 0.256 \text{ rad/s} \quad (28)$$

This results in:

$$T_d = 0.78 \text{ s} \quad (29)$$

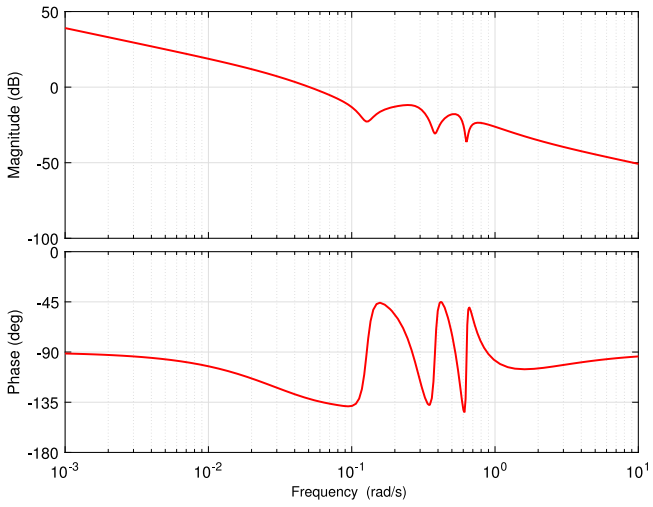

Fig. 14. Case Study A. Bode diagram of $L_a(s)$.

$$T_f = 15.6 \text{ s} \quad (30)$$

As far as $R_{pi}(s)$ is concerned, since $\mu_g = -0.0193$ m and $T_p = 16$ s, it is possible to adopt the pole compensation approach and require $\omega_c = 0.0895$ rad/s. To this end, one can set:

$$T_i = T_p = 16 \text{ s} \quad (31)$$

$$\mu_r = -4.6392 \text{ m}^{-1} \quad (32)$$

This tuning provides a phase margin $\phi_m = 47.93°$ and a gain margin $K_m = \infty$. In addition, it is possible to note from the Bode diagram of $L(s)$ that the highest resonance peak reaches −12 dB of magnitude: as discussed in Galuppini et al. (2020), the de-amplification of the resonance peaks can be beneficial both in terms of robustness and cost of control.

Finally, the parameters of $GS - \alpha$ are set as follows:

$$\alpha^* = 0.55 \quad (33)$$

$$\mu^*_{ratio} = 0.1 \quad (34)$$

$$p = 4 \quad (35)$$

5.1.2. Simulation results

The performances of control algorithm designed in this Section is now assessed by means of a set of simulations, as described in Section 2. In particular, Table 1 reports the values of the performance metrics for each demand offset value. The regulation error ranges from 0.81 [m] and decreases as the demand offset increases, with a minimum value of 0.49 [m]. The cost of control shows an opposite behaviour, increasing as the demand offset increases, from its lowest value (15.5), to the highest (28.2). Fig. 15 depicts results for a whole day simulation with the standard demand profile.

5.2. Case study B

The application of the proposed methodology to Case Study B is discussed in detail in this Section (see Eq. (36) in Box II).

$$G_b(s) = \frac{-0.001812s^8 + 0.0002487s^7 - 0.002848s^6 - 0.0009737s^5 - 0.0003301s^4 - 7.241 \times 10-05s^3 - 8.275 \times 10-06s^2 - 1.013 \times 10-06s - 2.124 \times 10-08}{s^9 + 0.2841s^8 + 0.5369s^7 + 0.1105s^6 + 0.06009s^5 + 0.0083s^4 + 0.002042s^3 + 0.0001617s^2 + 1.69 \times 10-05s + 3.369 \times 10-07} e^{-19s} \quad (36)$$

Box II.

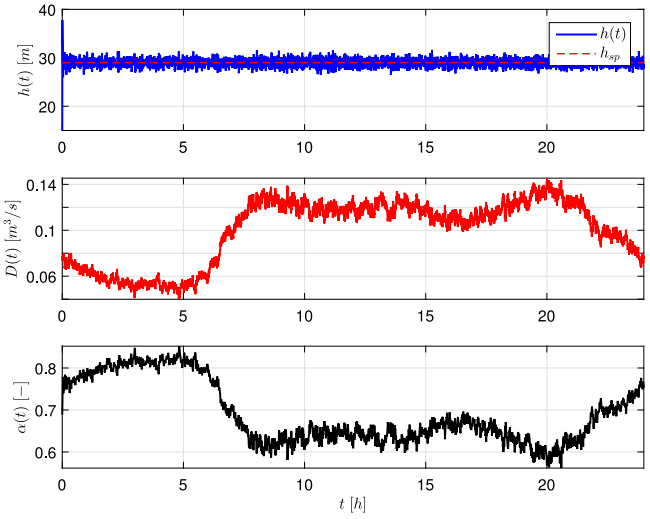

Fig. 15. Case Study A: closed-loop simulation with $FPI - SP - gs$ and no demand offset. Top: pressure $h(t)$ and pressure setpoint h_{sp}. Middle: demand $D(t)$. Bottom: valve closure $\alpha(t)$.

Table 1
Case Study A: performance of $FPI - SP - gs$ algorithm (ω_c = 0.0895 rad/s), for different demand offsets.

Demand Offset [m³/s]	$\sum \lvert\Delta\alpha\rvert$ [–]	$Mean\lvert e(k)\rvert$ [m]
−0,03	15.5	0.81
−0,02	15.4	0,69
−0,01	17.7	0.61
0	19.5	0.56
0,01	21.9	0.52
0,02	24.9	0.5
0,03	27.3	0.48
0,04	28.3	0.48
0,05	28.2	0.49

5.2.1. Nominal design and gain scheduling policies

The control goal in Case Study B is pressure regulation at h_{sp} = 25 m at node 1, which is chosen as controlled node. Recall that the average value of each demand $D_i(t)$ is the same for demand profiles A and B, therefore a single working point WP_B can be defined for Case Study B:

$$WP_B = \begin{cases} \overline{\xi} = 170.45 \ (i.e.\ \overline{\alpha} = 0.619) \\ \overline{H} = 39.6 \text{ m} \\ \overline{D}_1 = 0.0014 \text{ m}^3/\text{s} \\ \dots \\ \overline{D}_{N_{nodes}} = 0.0007 \text{ m}^3/\text{s} \\ \overline{h} = 25 \text{ m} \\ \overline{Q} = 0.0586 \text{ m}^3/\text{s} \end{cases} \quad (37)$$

A step response simulation around WP_B allows to obtain the input–output data for the identification of $G_b(s)$. Fig. 16 shows the identification data and the corresponding prediction obtained from $G_b(s)$, whose Bode diagram is depicted in Fig. 17. The complete definition of $G_b(s)$ is reported in Eq. (36). Recall that, for case Study A, the pure delay is given by the time required by the pressure wave generated from the valve to reach the pressure sensor. For Case Study B, such pressure wave results in a number of waves that reach the sensor through many possible paths, and the value of the delay coincides with the time required by the wave to travel along the *quickest path*, which can be computed based on the knowledge of WDS topology. In this particular case, the delay τ_b results:

$$\tau_b = 19 \text{ s} \quad (38)$$

Based on $G_b(s)$, a Smith predictor is designed to compensate for the effect of the pure delay in the design of the nominal loop function $L_b(s)$, whose Bode diagram is depicted in Fig. 18.

$R_f(s)$ is first defined by deriving ω_{rp} from $G_b(s)$:

$$\omega_{rp} = 0.1 \text{ rad/s} \quad (39)$$

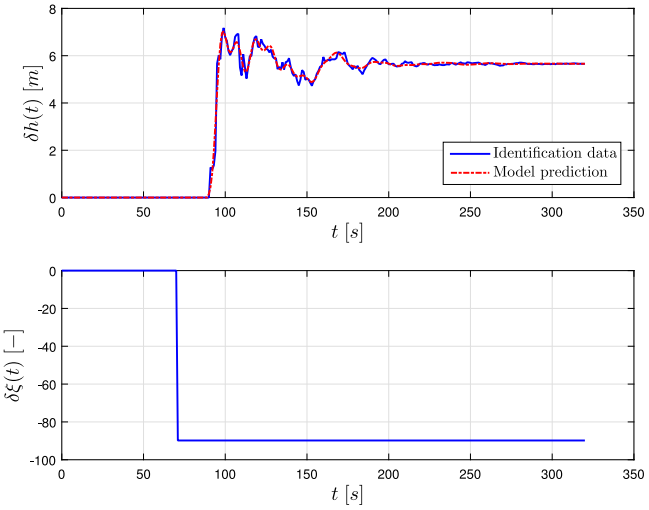

Fig. 16. Case Study B: model identification. Top: pressure variation $\delta h(t)$ (blue, solid line: identification data; red, dashed line: model prediction). Bottom: valve head loss coefficient variation $\delta\xi(t)$.

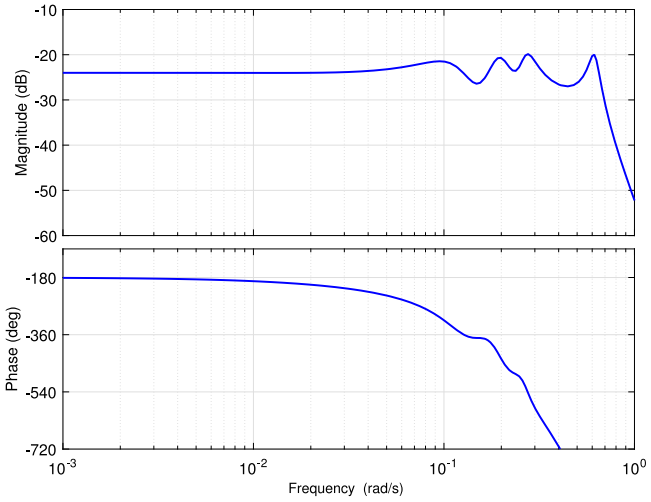

Fig. 17. Case Study B. Bode diagram of $G_b(s)$.

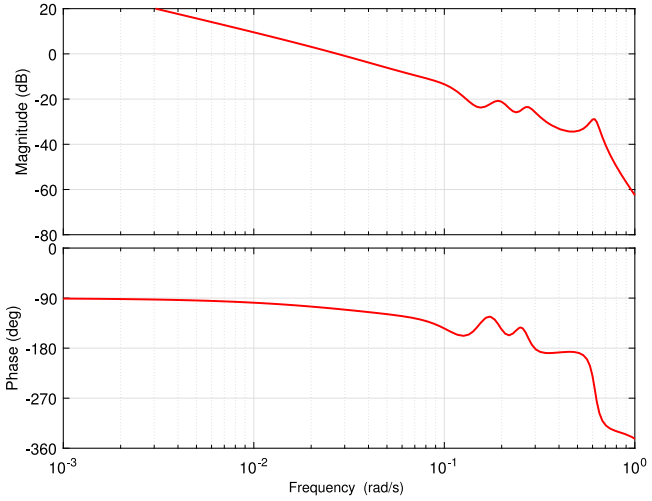

Fig. 18. Case Study B. Bode diagram of $L_b(s)$.

Table 2
Case Study B: performance of $FPI-SP-gs$ ($\omega_c = 0.0309$ rad/s) with demand profiles A and B.

Demand Profile	$\sum\lvert\Delta\alpha\rvert$	$Mean\lvert e(k)\rvert$
	[−]	[m]
A	8.9	0.76
B	9.2	0.67

This results in:

$$T_d = 2 \text{ s} \tag{40}$$

$$T_f = 40 \text{ s} \tag{41}$$

From the analysis of $G_b(s)$, it holds that $\mu_g = -0.0631$ m. By requiring $\omega_c = 0.0306$ rad/s, it is possible to get to:

$$\mu_r = -0.4849 \text{ m}^{-1} \tag{42}$$

In addition, note that T_p is not defined, since all the poles of the transfer function are complex conjugate. In this case, the integral time constant T_i can be treated as a free design parameter to shape the loop function and adjust the phase margin. The choice adopted in this work for T_i is:

$$T_i = 5.5 \text{ s} \tag{43}$$

This tuning provides a phase margin $\phi_m = 70°$ and a gain margin $K_m = 18.9$. Moreover, the analysis of Bode diagram of $L(s)$ shows that the highest resonance peak reaches −15 dB of magnitude.

Finally, the parameters of $GS-\alpha$ are set as follows:

$$\alpha^* = 0.5 \tag{44}$$

$$\mu^*_{ratio} = 0.1 \tag{45}$$

$$p = 6 \tag{46}$$

5.2.2. Simulation results

For Case Study B, the performances of $FPI-SP-gs$ algorithm are evaluated by means of a two simulations, characterised by two different demand patterns. The values of the performance metrics for each demand profile are reported in Table 2.

Figs. 19 and 20 depicts results for a whole day simulation with demand profile A and B, respectively. Note that, for demand profile A, $GS-\alpha$ has no effect since $\alpha(t) > \alpha^*$ always holds. On the contrary, it has great importance in case of demand profile B, since it reaches high values that force the control valve to reach very open positions, and

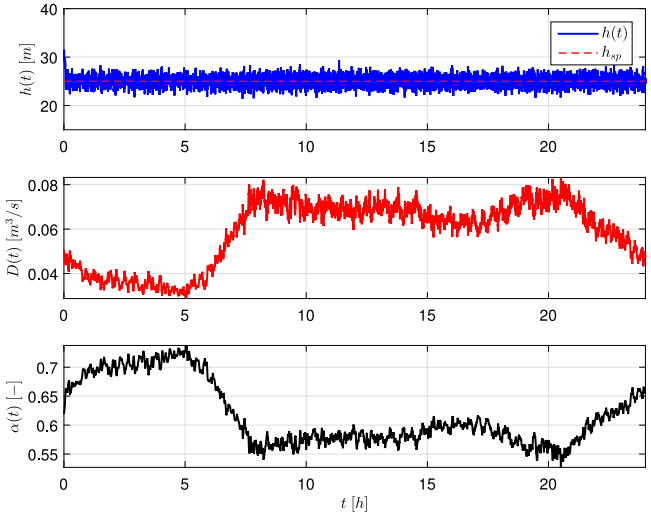

Fig. 19. Case Study B: closed-loop simulation with $FPI-SP-gs$ and demand profile A. Top: pressure $h(t)$ and pressure setpoint h_{sp}. Middle: demand $D(t)$. Bottom: valve closure $\alpha(t)$.

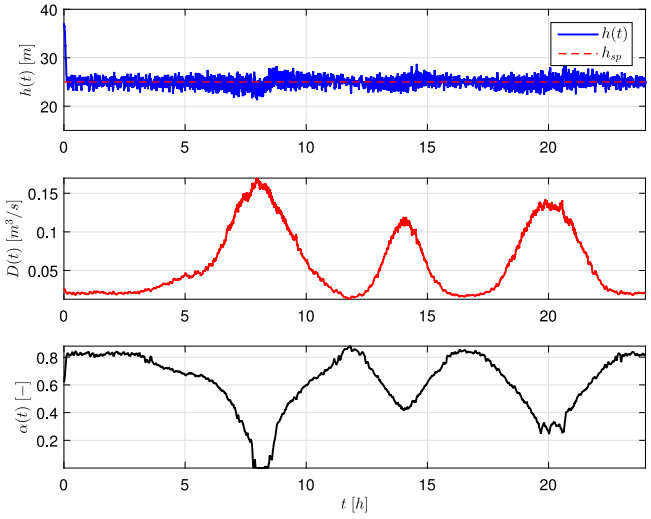

Fig. 20. Case Study B: closed-loop simulation with $FPI-SP-gs$ and demand profile B. Top: pressure $h(t)$ and pressure setpoint h_{sp}. Middle: demand $D(t)$. Bottom: valve closure $\alpha(t)$.

saturation (completely open). For sake of comparison, the simulation was repeated by disabling $GS-\alpha$ (let this algorithm be denoted as $FPI-SP-gsQ$), and the results plot in Fig. 21. This allows highlighting the benefit of the additional gain scheduling policy, which reduces the valve movements without degrading too much the regulation error when the valve reaches the almost flat region of its $\xi(\alpha)$ characteristic curve. Note that, with without $GS-\alpha$, and in case of $\alpha \approx 0$, the valve speed limit was reached for some instants. This suggests that $GS-\alpha$ can be a useful tool to reduce problems related to valve speed saturation, which may occur at very high flow values. However, it must be remarked that, in case of a sensibly lower valve speed, or a faster system dynamics which may allow for wider closed-loop bandwidths, it may be necessary to rely on more complex control designs to explicitly account for the valve speed limit.

6. Discussion of results

The $FPI-SP-gs$ control algorithms described in this work was successfully tested in two case studies characterised by different

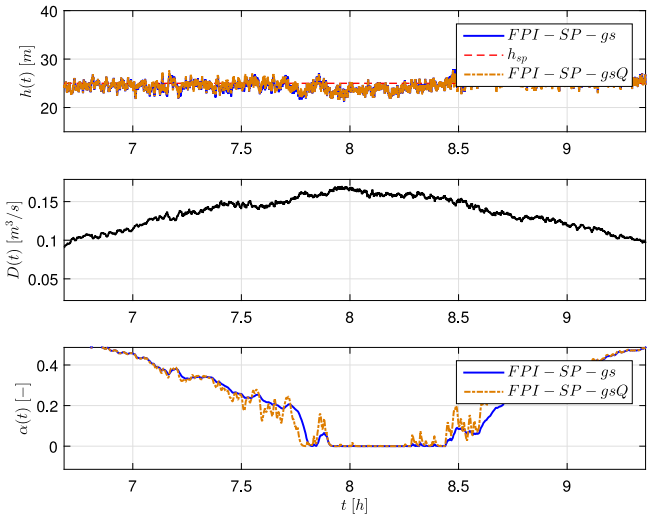

Fig. 21. Case Study B: detail of closed-loop simulation with $FPI-SP-gs$ (blue, solid line) and $FPI-SP-gsQ$ (orange, dashed line) and demand profile B. Top: pressure $h(t)$ and pressure setpoint h_{sp}. Middle: demand $D(t)$. Bottom: valve closure $\alpha(t)$.

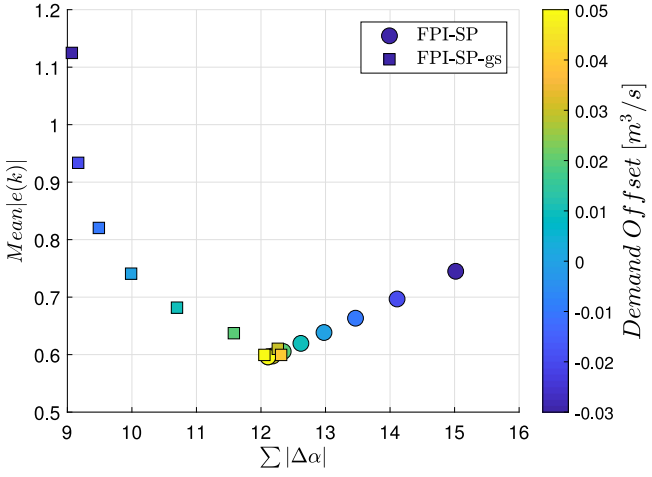

Fig. 22. Case Study A: results of closed-loop simulations with $FPI-SP$ (circles) and $FPI-SP-gs$ (squares), with $\omega_c = 0.0314$ rad/s and different demand offsets.

dynamic behaviours. The dynamics of Case Study A, a water distribution system with a simple topology, is in fact dominated by the water hammer effect. On the contrary, in case of Case Study B, the dynamics is mainly determined by its complex topology. In both cases the control algorithm provided satisfactory results all over a wide range on operating conditions, with demand values spreading from very low values to very high ones. Despite this variety of operating points and the large closed-loop bandwidth required in the design of the loop function, no instability even was faced in simulations, thus demonstrating the robustness of the approach.

To further investigate the benefits of the $FPI-SP-gs$ approach, a comparison with previous studies is now introduced, starting from Case Study A. In particular, reference is made to the $FPI-SP$ algorithm introduced in Galuppini et al. (2019). The $FPI-SP$ algorithm shares the same design rationale described in Section 4.1.3, but directly relies on $\alpha(t)$ as control variable, without any gain scheduling policy.

For this comparison, the $FPI-SP$ algorithm is tuned to obtain the same loop function as obtained in the nominal design of the $FPI-SP-gs$ algorithm. While nominal stability of the $FPI-SP$ algorithm was proved by means of the *Bode criterion* (Seborg et al., 2010), when applied to the system, the algorithm makes the closed-loop unstable as

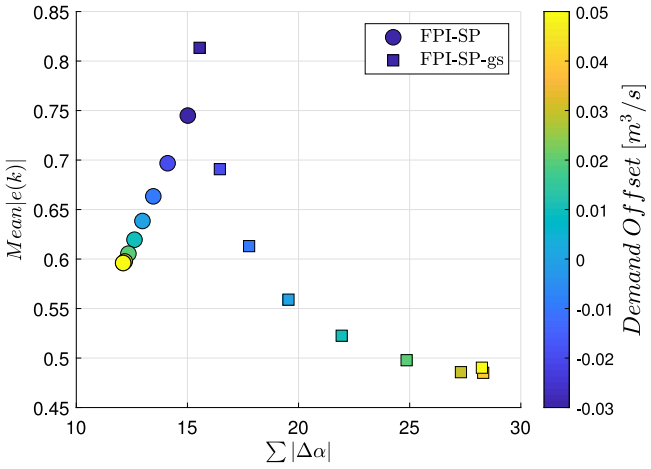

Fig. 23. Case Study A: results of closed-loop simulations with $FPI-SP$ ($\omega_c = 0.0314$ rad/s) (circles) and $FPI-SP-gs$ ($\omega_c = 0.0895$ rad/s) (squares), with different demand offsets.

Table 3
Case Study A: performance of $FPI-SP$ algorithm ($\omega_c = 0.0895$ rad/s), for different demand offsets.

Demand Offset [m^3/s]	$\sum\|\Delta\alpha\|$ [–]	$Mean\|e(k)\|$ [m]
–0,03	838.4	3.24
–0,02	838.9	3.24
–0,01	837.9	3.19
0	836.1	3.11
0,01	830.9	2.99
0,02	818.26	2.83
0,03	773.7	2.58
0,04	622.67	2.09
0,05	437.1	1,59

soon as the system moves away from the nominal WP. The valve speed saturation avoids that instability results in diverging oscillations, but produces persistent oscillations of both the pressure $h(t)$ and the valve closure $\alpha(t)$. Consequently, both the regulation error and the cost of control assume unacceptably high values, as reported in Table 3.

A trial and error tuning of the $FPI-SP$ algorithm, performed directly on the simulated plant, allowed to define the required closed-loop bandwidth $\omega_c = 0.0314$ rad/s as the widest admissible one, for Case Study A. The $FPI-SP-gs$ control algorithm is then retuned by requiring the same closed-loop bandwidth. Fig. 22 shows a comparison of the results obtained with $FPI-SP$ and $FPI-SP-gs$ algorithms, both tuned with $\omega_c = 0.0314$ rad/s. The cost of control is reported on the abscissa and the regulation error on the ordinate. The marker colour indicates the demand offset used for the simulation. Note that, for negative demand offsets, the $FPI-SP$ algorithm produces lower errors and higher costs. For positive demand offsets the performances of the two control algorithms get similar.

These results are consistent with the nonlinearity analysis performed in Galuppini et al. (2020): if α is adopted as control variable, when the demand decreases and $\alpha(t)$ increases, the process gain increases due to the $\xi(\alpha)$ relation. While for intermediate values of $\alpha(t)$ this effect is partially compensated by the gain decrease due to the decrease in $Q(t)$, when $\alpha(t)$ gets close to 1, this may result in instability of the closed-loop. On the other hand, for high demand values, $\alpha(t)$ moves to the flat region of the $\xi(\alpha)$ curve, resulting in a decrease of the process gain and eventually of the closed-loop bandwidth.

To conclude the analysis for Case Study A, it is possible to compare the results obtained with $FPI-SP-gs$ algorithms as originally tuned (i.e. $\omega_c = 0.0895$ rad/s) to those obtained with the $FPI-SP$ algorithm with the widest closed-loop bandwidth possible (i.e. $\omega_c = 0.0314$ rad/s).

Table 4
Case Study B: performance of $FPI-SP$ algorithm ($\omega_c = 0.0309$ rad/s) with demand profiles A and B.

Demand Profile	$\sum \lvert\Delta\alpha\rvert$	$Mean\lvert e(k)\rvert$
	[−]	[m]
A	11.4	0.74
B	9.6	0.62

The results of simulations are reported in Fig. 23. In this case the control error obtained with $FPI-SP-gs$ algorithm is always lower than that of $FPI-SP$ algorithm, with the only exception of the simulation with demand offset set at −0.03 m^3/s, at the price of a higher cost of control.

A final remark about $FPI-SP-gs$ algorithm is related to its performances at high demand values. With reference to Figs. 22 and 23, as the demand offset grows higher, the points tend to concentrate in a smaller region. This is due to the effect of $GS-\alpha$, which progressively reduces the closed-loop bandwidth to avoid excessively high costs of control, not justified by a small improvement in the regulation error.

Let now consider the results obtained with $FPI-SP$ and $FPI-SP-gs$ algorithms with simulation of Case Study B. Again, the two control algorithms are tuned by requiring the same nominal loop function, with $\omega_c = 0.0306$ rad/s, as discussed in Section 5.2. In particular, Table 4 reports the values of the performance metrics for $FPI-SP$ algorithm, while Table 2 those of $FPI-SP-gs$ algorithm. In case of demand profile A, $FPI-SP-gs$ clearly outperforms $FPI-SP$ by providing a similar regulation error with a strongly reduced cost of control. On the other hand, with demand profile B, the performances of the two algorithms are very similar.

This comparison further stresses the benefits of introducing the presented gain scheduling approach in the design of the RTC algorithm. As a matter of fact, a more robust control design typically results in reduced performances, especially in terms of regulation error. In this case instead, the introduction of gain scheduling policies allows making the overall control design more robust, and in turn reducing the regulation error (as in Case Study A), or rather obtaining a similar regulation error at lower cost of control (as in Case Study B, demand profile A). Furthermore, the $FPI-SP-gs$ algorithm did not require any trial and error tuning procedure, since the model-based design provided good performances when applied to the nonlinear system. On the other hand, a trial and error tuning procedure can be required for the $FPI-SP$ algorithm, which resulted in closed-loop instability when the model-based design was tested on the nonlinear system in Case Study A. In this respect, it must be underlined that a trial and error tuning procedure on a real plant would last several days and possibly result in inconvenience for the users. It may also stress the water distribution infrastructure in case of instability events. Therefore a control algorithm which requires no or very little retuning on the real plant is preferable.

7. Conclusion

This paper proposed a frequency domain control design with a gain scheduling approach to improve real time pressure control in water distribution networks. The algorithm was extensively tested with simulations on a numerical model of the WDN. In particular, two different topologies and different demand profiles were considered, to assess its performances over a wide range of situations. The algorithm delivered satisfactory results, and detailed comparison with a simpler class of frequency domain control algorithms from Galuppini et al. (2019) underlined the benefits of the new approach. In fact, this work demonstrates that a careful choice of the control variable, together with a nonlinearity inversion block and a gain scheduling policy based on physical considerations, allow compensating for the main nonlinearities of the process. The robustness margins required by the nominal design of the regulator can therefore be reduced, thus leading to wider closed-loop bandwidths and improved regulation error. Notably, the new approach did not require any retuning when applied to the nonlinear system. This represents a clear advantage since operations on the plant may require time and result in inconvenience for the users. Finally, this paper demonstrates that a further gain scheduling policy can be introduced to balance between regulation error and cost of control, as the system moves through different working points, extending in this way the actuator lifetime without degrading too much the regulation performances of the control scheme.

As a concluding remark, it should be noted that the control problem faced in this work can also be tackled with the tools of robust control based on Linear-Parameter-Varying (LPV) systems theory, to address in a more rigorous manner the topic of LPV stability (Blanchini, Casagrande, Giordano, & Miani, 2015; Shamma, 2012; Stewart, 2012). Other interesting possibilities include Adaptive Control (Narendra & Annaswamy, 2012), and Model Predictive Control (Magni & Scattolini, 2014), which allows facing the problem in a multivariable context, where a single valve is available to regulate pressure at multiple WDN nodes, while explicitly considering the physical constraints acting on the control action. The analysis of such control techniques is left as future work.

Declaration of competing interest

The authors declare that they have no known competing financial interests or personal relationships that could have appeared to influence the work reported in this paper.

References

Blanchini, F., Casagrande, D., Giordano, G., & Miani, S. (2015). On the lpv control design and its applications to some classes of dynamical systems. In *Developments in Model-Based Optimization and Control* (pp. 319–338). Springer.

Campisano, A., Creaco, E., & Modica, C. (2009). Rtc of valves for leakage reduction in water supply networks. *Journal of Water Resources Planning and Management*, *136*(1), 138–141.

Campisano, A., Modica, C., Reitano, S., Ugarelli, R., & Bagherian, S. (2016). Field-oriented methodology for real-time pressure control to reduce leakage in water distribution networks. *Journal of Water Resources Planning and Management*, *142*(12), Article 04016057.

Campisano, A., Modica, C., & Vetrano, L. (2011). Calibration of proportional controllers for the rtc of pressures to reduce leakage in water distribution networks. *Journal of Water Resources Planning and Management*, *138*(4), 377–384.

Cembrano, G., Wells, G., Quevedo, J., Pérez, R., & Argelaguet, R. (2000). Optimal control of a water distribution network in a supervisory control system. *Control Engineering Practice*, *8*(10), 1177–1188.

Ciaponi, C., Franchioli, L., Murari, E., & Papiri, S. (2015). Procedure for defining a pressure-outflow relationship regarding indoor demands in pressure-driven analysis of water distribution networks. *Water Resources Management*, *29*(3), 817–832.

Creaco, E. (2017). Exploring numerically the benefits of water discharge prediction for the remote rtc of wdns. *Water*, *9*(12), 961.

Creaco, E., Campisano, A., Franchini, M., & Modica, C. (2017). Unsteady flow modeling of pressure real-time control in water distribution networks. *Journal of Water Resources Planning and Management*, *143*(9), Article 04017056.

Creaco, E., Campisano, A., & Modica, C. (2018). Testing behavior and effects of prvs and rtc valves during hydrant activation scenarios. *Urban Water Journal*, *15*(3), 218–226.

Creaco, E., & Franchini, M. (2013). A new algorithm for real-time pressure control in water distribution networks. *Water Science and Technology: Water Supply*, *13*(4), 875–882.

Creaco, E., & Walski, T. (2017). Economic analysis of pressure control for leakage and pipe burst reduction. *Journal of Water Resources Planning and Management*, *143*(12), Article 04017074.

Farley, M., & Trow, S. (2003). *Losses in water distribution networks*. IWA Publishing.

Fontana, N., Giugni, M., Glielmo, L., Marini, G., & Verrilli, F. (2017). Real-time control of a prv in water distribution networks for pressure regulation: Theoretical framework and laboratory experiments. *Journal of Water Resources Planning and Management*, *144*(1), Article 04017075.

Fontana, N., Giugni, M., Glielmo, L., Marini, G., & Zollo, R. (2017). Real-time control of pressure for leakage reduction in water distribution network: Field experiments. *Journal of Water Resources Planning and Management*, *144*(3), Article 04017096.

Galuppini, G., Creaco, E., Toffanin, C., & Magni, L. (2019). Service pressure regulation in water distribution networks. *Control Engineering Practice*, *86*, 70–84.

Galuppini, G., Magni, L., & Creaco, E. (2020). Stability and robustness of service pressure regulation in water distribution networks. *Journal of Hydraulic Engineering*, *146*(4), 04020023.

Grosso, J. M., Maestre, J. M., Ocampo-Martinez, C., & Puig, V. (2014). On the assessment of tree-based and chance-constrained predictive control approaches applied to drinking water networks. *IFAC Proceedings Volumes*, *47*(3), 6240–6245, 19th IFAC World Congress.

Grosso, J., Ocampo-Martínez, C., Puig, V., & Joseph, B. (2014). Chance-constrained model predictive control for drinking water networks. *Journal of Process Control*, *24*(5), 504–516.

Grosso, J. M., Velarde, P., Ocampo-Martinez, C., Maestre, J. M., & Puig, V. (2017). Stochastic model predictive control approaches applied to drinking water networks. *Optimal Control Applications & Methods*, *38*(4), 541–558.

Janus, T., & Ulanicki, B. (2017). *Hydraulic modelling for pressure reducing valve controller design addressing disturbance rejection and stability properties*. Elsevier.

Janus, T., & Ulanicki, B. (2018). Improving stability of electronically controlled pressure-reducing valves through gain compensation. *Journal of Hydraulic Engineering*, *144*(8), Article 04018053.

Lambert, A., Fantozzi, M., & Thornton, J. (2013). Practical approaches to modeling leakage and pressure management in distribution systems–progress since 2005. In *Proceedings of the 12th int. conf. on computing and control for the water industry-CCWI2013*.

Ljung, L. (1991). *System identification toolbox: For use with MATLAB: user's guide*. Math Works.

Magni, L., & Scattolini, R. (2014). *Advanced and Multivariable Control*. Pitagora.

Narendra, K. S., & Annaswamy, A. M. (2012). *Stable Adaptive Systems*. Courier Corporation.

Ocampo-Martinez, C., Barcelli, D., Puig, V., & Bemporad, A. (2012). Hierarchical and decentralised model predictive control of drinking water networks: Application to barcelona case study. *IET Control Theory & Applications*, *6*(1), 62–71.

Ocampo-Martinez, C., Puig, V., Cembrano, G., & Quevedo, J. (2013). Application of predictive control strategies to the management of complex networks in the urban water cycle [applications of control]. *IEEE Control Systems*, *33*(1), 15–41.

Pezzinga, G. (2000). Evaluation of unsteady flow resistances by quasi-2d or 1d models. *Journal of Hydraulic Engineering*, *126*(10), 778–785.

Seborg, D. E., Mellichamp, D. A., Edgar, T. F., & Doyle, F. J., III (2010). *Process dynamics and control*. John Wiley & Sons.

Shamma, J. S. (2012). An overview of lpv systems. In *Control of Linear Parameter Varying Systems with Applications* (pp. 3–26). Springer.

Stewart, G. E. (2012). A pragmatic approach to robust gain scheduling. *IFAC Proceedings Volumes*, *45*(13), 355–362.

Streeter, V. L., Wylie, E. B., & Bedford, K. W. (1998). *Fluid mechanics*. WCB.

Thornton, J., & Lambert, A. (2006). Managing pressures to reduce new breaks. *Water*, *21*(December 2006), 24–26.

Toro, R., Ocampo-Martínez, C., Logist, F., Impe, J. V., & Puig, V. (2011). Tuning of predictive controllers for drinking water networked systems. *IFAC Proceedings Volumes*, *44*(1), 14507–14512, 18th IFAC World Congress.

Van Zyl, J., & Cassa, A. (2013). Modeling elastically deforming leaks in water distribution pipes. *Journal of Hydraulic Engineering*, *140*(2), 182–189.

Walski, T. M., Chase, D. V., Savic, D. A., Grayman, W., Beckwith, S., & Koelle, E. (0000). Advanced water distribution modeling and management.